Fracture 1977, Volume 1, ICF4, Waterloo, Canada, June 19 - 24, 1977

FRACTURE RESEARCH IN THE MAX-PLANCK-INSTITUTE IN DUESSELDORF

A. Kochendoerfer*

ABSTRACT

THEORETICAL RESEARCH: By the transformation of the integral equation for the dislocation density in a slip plane inclined to the crack plane into a Fredholm equation a reliable numerical evaluation becomes possible. The results on the stress field, the crack tip displacement δ and the plastic zone size are in good agreement with the results obtained by finite element calculations. By an extension of the model, the influence of linear strain hardening on the σ, δ-curve and the relaxation of δ during unloading have been studied. Finally the model has been applied to the initiation and propagation of microcracks in structural steels at low temperatures.

EXPERIMENTAL RESEARCH: The σ, δ-curves of 2CT specimens of a mild steel with different a/W ratios have been measured at room temperature. The dependences of δ on σ/σ_{gy} and on a/W agree qualitatively well with those predicted by the theory of a linear sequence of equidistanced cracks with coplanar plastic zones. The results confirm the basic principle that the full scale yielding states are equivalent states and that correspondingly the curves σ/σ_{gy} versus δ/δ_{gy} have the same course up to general yielding. The consequences on the course of the curves normalized K_I versus normalized δ are discussed. Experiments are in progress at lower temperatures to examine the validity of the COD concept with respect to the influence of a/W as are experiments with small specimens to examine the possibility to evaluate K_{Ic} from small specimen data. The basic principles of the latter problem are outlined in this paper, and the results of both investigations shall be reported in the lecture.

1. INTRODUCTION

During the last years a research group for the study of fracture problems has been established in the Institute. It has consisted of P. Neumann, H. Reidel, H.D. Schulze, G. Bauer and myself and is complemented by several young men in post-graduate studies. I am pleased to be able to report on our work at this conference. This is especially the case because I shall retire from the scientific scene after the Conference. This lecture is therefore a farewell after a 40 years work in various fields of metal physics.

This paper first reports on the theoretical research of Riedel and then on the results of our experimental research and their interpretation. The extensive research of P. Neumann on the initiation and propagation of ductile fatigue cracks is omitted because the paper would then have become too long. On the other hand, Neumann has published several papers [1,2] and will report on his concepts elsewhere at this conference. Using the

*Department of Metal Physics, Max-Planck-Institut fuer Eisenforschung, Duesseldorf, Federal Republic of Germany.

recommended nomenclature, G is the shear modulus, numerical calculations are made for isotropic materials with $G = 8.10^4$ MPa, $\nu = 0.28$, and $E = 2.06 \cdot 10^5$ MPa. The abbreviation LEA stands for linear elastic approximation and SSY(R) for small scale yielding (range).

2. THEORETICAL INVESTIGATIONS ON A CRACK WITH INCLINED SLIP PLANES IN AN INFINITE BODY

2.1. No strain hardening

In the first approach of this problem the plasticity has been confined to zones coplanar with the crack plane [3,4,5]. Plastic yielding on inclined slip planes under plane strain tension has been treated with the T-stress approximation by Rice [6], numerically by Bilby and Swinden [7] and more exhaustively by Vitek [8]. There are, however, some difficulties in applying numerical methods to the singular integral equation governing the problem.

To avoid these difficulties, Riedel [9] has transformed this equation to a Fredholm integral equation which allows reliable numerical evaluations, and this transformation was indeed the most expensive step. Moreover, elastic anisotropy, rather general loading modes and yielding on one, two or four slip planes have been included. Figure 1 shows the used coordinate systems and the denotations. In the components of the stress tensor the indices 1 and 2 correspond to the coordinates x and y respectively. The applied stress σ^{∞}_{22} is termed by σ. The equilibrium condition is that the total shear stress acting at any point of a glide plane is zero:

$$\alpha \int_0^L \frac{\mathscr{D}(\eta')d\eta'}{\eta-\eta'} + \int_0^L \beta(\eta,\eta')\mathscr{D}(\eta')d\eta' + f(\eta)\delta$$

$$+ g(\eta)\sigma^{\infty}_{12} - \frac{\sin 2\theta}{2}\sigma_{11} + h(\eta)\delta_1 - \tau_o = 0 \qquad (1)$$

$\mathscr{D}(\eta)$ is the unknown dislocation density in a slip plane, L is the slip band length determined by $\mathscr{D}(\eta \geq L)=0$, σ^{∞}_{ij} ($\sigma^{\infty}_{22}=\sigma$) are the remotely applied stresses and τ_o is the frictional shear stress. For a Tresca material it is connected with the uniaxial yield stress σ_y by

$$\sigma_y = 2\tau_o \qquad (1a)$$

The first term in equation (1) describes the interaction between the dislocations in the considered slip plane. The second term contains the image stresses and the stresses originating in the other slip planes. The following three terms represent the actions of the applied stresses. The next term takes into account one sided plastic crack opening δ_1 of a wedge type crack which may be included in the analysis if slip occurs at one crack tip only. The functions α, β, f, g and h may be taken from the paper of Atkinson [10] for anisotropic elasticity.

Once $\mathscr{D}(\eta)$ has been determined from equation (1), paying regard to the boundary conditions, other elastic-plastic quantities such as the stresses σ_{ij}, the strains ε_{ij}, the crack tip opening displacement δ and the crack profile can be calculated by suitable integrations. Because of the complexity of the integral kernel $\beta(\eta,\eta')$ no closed form solution of equation (1) can be expected. Moreover, the singular term $1/(\eta-\eta')$ poses difficulties on the numerical analysis of the equation. Therefore, in the present

investigation equation (1) was transformed into a Fredholm integral equation by a method reported by Muskhelishvili [11]. This transformation is essentially an inverse Hilbert transformation. Replacing the integral by a sum for m discrete points

$$\eta_n = L\left(1-\cos\pi\frac{n-1/2}{m}\right)/2 \qquad n = 1,2,\ldots,m \qquad (2)$$

the Fredholm equation is converted into a set of m simultaneous linear equations which can be solved numerically. Since in equation (1) the stress σ^{∞}_{11} appears combined with τ_o only, τ_o may be replaced by $\tau^{*}_{o} = \tau_o + (\sin 2\theta)\,\sigma^{\infty}_{11}/2$. We retain the denotation τ_o, have in mind, however, that $\sigma^{\infty}_{11} \neq 0$ may be included in the results.

Detailed numerical calculation has been carried out for the tensile loading mode $\sigma = \sigma^{\infty}_{22} \neq 0$, $\sigma^{\infty}_{11} = \sigma^{\infty}_{12} = 0$, four slip planes and an isotropic material. In the following the results are shortly described and represented in the Figures 2 to 7.

(a) In the LEAR and in the T-stress approximation the present method confirms the solutions of Rice [6] within 2% in the most important range $45^0 \leq \theta \leq 70.5^0$. For $\theta \leq 20^0$ and $\theta \geq 90^0$ the results of Vitek [8] are better confirmed than those of Rice.

(b) For the most important range $45^0 \leq \theta \leq 70.5^0$ (see below) results in the T-stress approximation

$$L = \frac{1}{2}\sin^2\theta(1+\cos\theta)\quad(1+\frac{\sigma}{\tau_o}\sin 2\theta)\cdot L_D \qquad (3)$$

L_D is the LEA value according to the Dugdale model for a Tresca material in plane strain:

$$L_D = \frac{\pi}{32}\frac{K_I^2}{\tau_o^2}\,, \qquad K_I = \sqrt{\pi a}\;\sigma \qquad (3a,b)$$

In the generalized form of equation (3) (and likewise of equation (4)) σ is replaced by the negative T-stress for which Rice [6] has given the expressions for different geometries. For the present geometry is $T = \sigma^{\infty}_{11} - \sigma$. According to the complete numerical solution L is plotted in a proper unit versus σ/τ_o in Figure 2. If the preferred slip direction is defined by the maximum of L, it is $\theta = 70.5^0$ in the SSYR, decreases with increasing stress and approaches to $\theta = 45^0$ if σ approaches to $2\tau_o$ $\theta = 45^0 = \sigma_y$. We expect therefore that the behaviour of a polycrystalline material in large specimens is best described by the present results with $\theta = 70.5^0$ in the SSYR and with $\theta = 45$ at the approaching to general yielding which is reached for $\sigma = \sigma_y$ for the present specimen geometry. Correspondingly we take these values of θ in each of the both cases for the numerical calculations.

(c) In the mentioned range of θ results furthermore in the T-stress approximation

$$\delta = \frac{1}{2}\sin^3\theta\;(1+\cos\theta)\quad(1+\frac{\sigma}{2\tau_o}\sin 2\theta)\cdot\delta_D \qquad (4)$$

with

$$\delta_D = \frac{(1-\nu^2)}{2E}\,\frac{K_I^2}{\tau_o} \qquad (4a)$$

According to the complete numerical solution δ is plotted in a proper unit versus σ/τ_o in Figure 3. These results become more familiar in the SSYR if, taking into account equations (1a), (3b) and (4a), equation (4) is written in the form

$$\frac{\delta}{\varepsilon_y} = \frac{(1-\nu^2)}{2} \sin^3\theta \, (1+\cos\theta) \, (1+ \frac{\sigma}{\sigma_y} \sin 2\theta) \left(\frac{K_I}{\sigma_y}\right)^2 \qquad (5)$$

If we denote, as usual, the tangent or secant slope by $1/\beta$:

$$\frac{1}{\beta} = \frac{(K_I/\sigma_y)^2}{(\delta/\varepsilon_y)} \qquad (6)$$

we obtain numerically

$$1/\beta(\text{LEA}, \theta=70.5^0) = 1{,}95 \qquad (6a)$$

$1/\beta$ decreases with increasing σ/σ_y, at first according to the factor $(1+\sigma/\sigma_y \sin 2\theta)^{-1}$ and then according to higher powers of σ/σ_y.

(d) A remarkable feature of the results (3) and (4) is that the deviations from the LEA are of the third order of the stress. For a 10% deviation equation (5) gives

$$\frac{\sigma}{\sigma_y} = 0.16, \quad \frac{\delta}{a} = 4.10^{-2}\varepsilon_y \text{ for } \theta = 70.5 \qquad (7)$$

These values are more than one order of magnitude smaller than those reported in the literature, for instance by Smith [12], from the study of coplanar yielding. The reason for these differences is that models basing on the Dugdale model predict fourth order deviations in the stresses from the LEA, only.

(e) The crack profile is given by the distance Δu of the crack faces as a function of the length coordinate x. These curves for various glide band lengths L are shown in Figure 4. The near crack tip behaviour is

$$\Delta u - \delta \sim -(a-x)(\ell n(1-x/a))^r \quad (r \geq 1) \qquad (8)$$

A curve has therefore a vertical tangent at the crack tip x=a. It deviates, however, quickly from this tangent so that the vertical run into the crack tip is not distinctly pronounced if the scale covers the total length from x=0 to x=a. Nevertheless the increasing curvature with approaching to the crack tip illustrates the problems of the exact experimental determination of δ.

2.2 Linear strain hardening

The extension of the model to a linear strain hardening material imposes no difficulties. The frictional stress is then given by

$$\tau = \tau_o + \nu \gamma \qquad (9)$$

where γ is the shear strain in a glide plane. The δ, σ-curve in proper units for $\nu=0.72\ \tau_o$ is plotted in Figure 5 together with the curve for no

strain hardening ($\nu=0$) for $\theta=45^0$. According to the statements on the preferred slip direction these curves are considered to be correct at higher stress ratios σ/σ_y. From these calculations results the dependence of the initial slope $1/\beta$ on ν/τ_o as shown in Figure 6. This dependence shall be used in section 3.8.

2.3 Unloading behaviour

If after some monotonic loading up to a stress $\sigma=\sigma_{load}$ the stress becomes continuously removed, the σ, δ-curve does not follow to the loading curve. This irreversibility exists because the frictional stress changes its sign at the back movement of the dislocations. During unloading the most important back stress on a dislocation is the image stress. It is the greater the nearer a dislocation is at the crack tip. Consequently for small loading stresses and correspondently small slip band lengths a worthmentioning part of the dislocations moves back into the crack and diminishes the crack tip displacement. For larger loading stresses and slip band lengths the dislocations far away from the crack tip are not influenced by the image stress. They re-arrange by the other interactions, only, and the crack tip displacement becomes less diminished than for low loading stresses. The unloading curves drawn in Figure 5 exhibit these features quantitatively. They accentuate that the measurement of δ in unloading specimens is unreliable in the SSYR.

The endpoints of the unloaded curves are those at which the crack faces contact each other in the middle x=0 of the crack. This result is essential at cyclic stressing and shall be discussed elsewhere.

2.4 Propagation of Microcracks

In unnotched specimens of mild steels at low temperatures microcracks are frequently generated in grain boundary cementite films by slip or twin bands [13, 14, 15]. Cottrell [16] has studied the generation of such a wedge type crack, especially for the dislocation geometry of bcc metals. He has furthermore set-up the energy equation for an infinite, tensile loaded body containing such a crack including the effective specific surface energy γ. From the condition that the first derivative with respect to the crack length vanishes results that a generated microcrack grows steadily with increasing stress until it becomes unstable at the fracture stress $\sigma=\sigma_f$. The resulting equation for σ_f contains γ and the number n of crack dislocations. As a further relation Cottrell takes into account the equilibrium condition between $\sigma=\sigma_f$, n and the glide band length L [17,18]. This relation can, however, no longer be applied once the crack has been generated [19]. For this reason the results of Cottrell are not quantitatively true, but have provided at first a qualitatitively correct description of the influence of the grain size d on σ_f, if put L=d. The present model pays regard to the true interaction between the slip band dislocations and the crack. It seems therefore to be suitable for the treatment of the propagation of a wedge type microcrack of the length 2a generated by one or two slip or twin bands of the length L if an instability condition is added. Riedel [20] assumes this condition to be that in a critical distance $x=x_c$ from the crack tip the normal stress σ_{22} must take a critical value σ_c. The results are presented in Figure 7. The used coordinates are necessary if all variables shall be respected. From Figure 7 can be seen that for unnotched specimens the results describe qualitatively correct the influences of the test temperature, determined by τ_o, of the grain size,

d~L, and of the carbide film thickness, d$_C$~2a, on the fracture stress. A quantitative evaluation is in progress. The field with negative values of the abscissa becomes essential for compressive stresses $\sigma_1^* < 0$. These cases involve interesting problems on the stable and unstable crack propagation on which has been reported [20].

2.5 Discussion

The present model with singular inclined slip planes will be best applicable to single crystals, in which plasticity has been observed to be restricted to narrow bands, Neumann [2], Pelloux [21]. Its applicability to polycrystalline materials may be tested by comparison of its results with those of finite element calculations. Larsson and Carlsson [22] have made such calculations with a modified boundary layer model for different specimen geometries. For a centre cracked large specimen their solution for δ agrees with the present solution for $\theta=70.5$ within less than 10% for $\sigma/\sigma_Y \gtrsim 0.25$. For smaller stresses the differences become larger than 20%. For such stresses a refined finite element calculation of Rice and Tracey [23] has given for a v. Mises material

$$1/\beta(\mathrm{LEA}) = 2.03 \qquad (10)$$

This value agrees with the value (6a) within 4%. It would be possible to reduce these differences by calculating $1/\beta$ according to equation (5) for a v. Mises material and by changing somewhat the preferred value of θ, but this seems not to be adequate since the differences have no practical significance.

From these considerations can be concluded that the present method is well fit for the treatment of the problems of cracks with plastic zones. Additionally to the questions already mentioned in this paper, others shall be studied in future.

3. INFLUENCE OF a/W ON THE YIELDING PROPERTIES

3.1 Preliminary remarks

In an earlier investigation [24] we have measured the flow stress $\sigma(\delta)$, belonging to a certain notch opening δ, for notched bending specimens of an annealed mild steel. We have then studied the fracture behaviour under the viewpoint that each $\sigma(\delta)$, T-curve ends at the occurence of the fracture at the temperature $T=T(\delta)$ for which $\sigma(\delta) = \sigma_f(\delta)$ for the value of δ in consideration. The interpretation of the results [25] was done by means of the theory of Cottrell [16].

For the investigations on which shall be reported here, we have used 2CT specimens with different ratios a/W. These allow for an evaluation of δ and of K_{Ic} and enable a reliable examination of the validity of the COD concept with respect to a/W. Because of some difficulties that arose at the machining of the deep slits and at the testing of the specimens with short crack lengths and high loading forces we could only measure the σ, δ-curves at room temperature until the deadline of the manuscript. These results provide interesting insights into the influence of a/W on the yielding properties that they are valuable themselves. The experiments on the fracture behaviour are in progress, on their results shall be reported at the ICF4 lecture.

The concepts and results are at first presented without comment, their discussion occurs in section 3.8.

3.2 Steel and specimens

The investigated steel was a mild killed steel R St 37-2 with a grain size of 26µm. Its yield stress at room temperature is σ_Y = 237 MPa. The specimens were 2CT specimens with W=100 mm and B~50 mm, but with a/W = 0.32, 0.53 and 0.69. The fatigue crack was produced according to the ASTM recommendations.

3.3 Evaluation of the nominal stress

As a measure of the loading force P we take the nominal stress σ defined as the stress with a constant absolute value over the ligament which provides the applied load P and/or the bending moment M [26]. For three point, 3PB, and four point, 4PB, bending specimens it is given by

$$\sigma(3PB) = \sigma(4PB) = \frac{4M}{B(W-a)^2} \qquad (11a,b)$$

and for CT specimens by

$$\sigma(CT) = \frac{P}{B(W-a)^2}\left\{(W+a) + \left[2(W^2+a^2)\right]^{1/2}\right\} \qquad (11c)$$

Frequently the nominal stress is defined as the maximum stress for a linear stress distribution. This stress is (for CT specimens about) 1.5 times greater than that used here.

3.4 General yield stress, constraint factor

The general yield stress σ_{gy} we have determined in the following way. For the bending specimens [24] we have measured the curves σ versus the bending angle. This angle is such an insensitive measure of the plastic deformation that it is detected only if general yielding has been reached. The stress-angle curve exhibits therefore a sharp bend-off from the apparently elastic part. The kink in the curve determines σ_{gy}. With this value we have obtained the value $V_{s,gy}$ of the surface displacement V_s from the curve σ versus V_s where V_s is measured with a high sensitive clip gauge device. For large specimens, e.g. CT specimens, this method of determining σ_{gy} and $V_{s,gy}$ is likewise applicable though the plastic deformations before general yielding are larger than in small specimens. The results are shown in Figure 8. The curves on the left hand side, upper abscissa scale, are recorded with a low sensitive device. The kink is not so sharp as with small specimens but well marked for a/W=0.53 and 0.69, less well marked for a/W=0.32. The curves on the right hand side, lower abscissa scale, have been obtained by recording V_s with a high sensitive device. From them are obtained the values of $V_{s,gy}$ with the values of σ_{gy} taken from the curves on the left hand side. $V_{s,gy}$ is nearly independent of the scatter of σ_{gy} for different specimens. The values of σ_{gy} and $V_{s,gy}$ marked by the points and the corresponding curves $\sigma=\sigma(V_s)$ are used furthermore. It is to be seen from the curves on the

right hand side that general yielding takes place just at the point beyond which a σ, V_S-curve becomes nearly straight with a low slope. This viewpoint becomes yet clearer in Figure 14.

Several specimens have been covered with a cracking-lacquer in order to observe the spreading of the plastic zone (Figure 9). The lacquer has the tendency to crack along normal stress lines but likewise along slip lines because of the shear deformations. At sufficiently low loads the second tendency prevails and the slip lines are well marked in the small scale and in the partial scale yielding range. The photographs of the former range are proper for a visual observation but not for a reproduction in this paper because the slip lines are too fine and weak. In Figure 9a, therefore, is a reproduced photograph of the partial scale yielding range. At general yielding slip lines and normal stress lines appear and especially the singular slip lines running to the opposite specimen surface (Figure 9b). It is possible that the singular lines are not to be seen in the reproduction. The values of σ_{gy} and $V_{S,gy}$ determined in this way agree with those obtained from the stress-displacement curves within some differences. These are caused by the uncertainty in observing the first singular slip lines. In the macroscopic deformation range the individual slip lines disappear in a uniform brightening of the plastic zone. In this range the crack opens considerably without to propagate (Figure 9c). The propagation begins deep in this range by the generation of a new crack at the tip of the opened fatigue crack (Figure 9d). Further features of the crack opening shall be considered in the next section.

As in our earlier paper [26] we define the constraint factor b_{gy} at general yielding by

$$b_{gy} = \sigma_{gy}/\sigma_y \qquad (12)$$

Its values for the used values of a/W are given in Table 1.

3.5 Evaluation of the crack tip displacement

δ has been evaluated with the equations derived by Schmidtmann, et al [27,28] from optical measurements of the crack profile in bending specimens. For the calculation of the V, x-curve (x = distance from the crack tip) for a given load the values of two displacements V_1 and V_2 in the distances $x=x_1$ and $x=x_2$ are necessary. In Figure 10 several V, x-curves are drawn. The measured points for $x=x_1$ are marked. The points for $x=x_2=x_S$ lie outside the Figure. The crack tip displacement is $\delta=V(x=0)$.

The curves run nearly linearly towards x=0. This course does not correspond to that in Figure 4 and also not to that obtained by Schmidtmann. The reason is that the exponent H in Schmidtmann's equation takes values between 0.95 and 1 for our measured values of V_1 and $V_2=V_S$ whereas it takes a value of about 0.75 in the measurements of Schmidtmann, et al [27]. The crack profile according to our photographs, observed in a microscope, is, however, a trapezium profile with rather straight basis and side lines. This can be seen from the photographs in Figure 9 for the larger openings. The displacement values measured in this way as soon as possible are marked in Figure 10. On the surfaces of some specimens we have made microindentations and measured their displacements. The values obtained in this way are marked in Figure 10, too. This method shall be refined and the measurements shall be extended until the crack tip. Since the present measurements confirm the results of the calculation, we consider

the evaluated values of δ to be reliable and the method of Schmidtmann, et al., to be applicable to CT specimens.

δ versus V_S is plotted in Figure 11. The curve exhibits the well known feature that the crack tip opening initially increases slowly compared with the surface opening until both varaibles increase equally. For the nearly linear part

$$\delta = -\kappa + \lambda V_S \qquad (13)$$

result of numerical values κ=0.09 mm, λ=0.13. For the curve of Schmidtmann and Ruf [28] is κ=0.09 mm, λ=0.26. Fields and Miller [29] have measured δ by means of replicas of a hardening silicon rubber for bending specimens and obtained κ=0.07 mm, λ=0.4. In all three cases κ has about the same value but λ differs. This has the consequences that the limit value

$$(v_S/\delta)_\infty = 1/\lambda \quad \text{for } V_S >> \kappa/\lambda \qquad (13a)$$

differs likewise. It takes the values 7.7, 3.8 and 2.5 in the above sequence. A finite element calcualtion of Egan [30] for CT specimens with a/W=0.5 has given the value 5.6. We shall yet examine the influence of a/W in order to state the degree of agreement of our values with that of Egan. Generally the results show that the limit values cannot be transmitted from one to another geometry.

3.6 Stress-displacement curves

We put on before some theoretical results on the dependence of δ on a/W for an infinite body containing a sequence of cracks of length 2a and distance 2W. For a mode III loading the middle planes are stress free and the results can be used for specimens of the length W with a surface crack of the length a. For a mode I loaded body this does not strongly hold but the results prove to be useful for the interpretation of the experimental results. We use the theoretical results of Bilby and Swinden [7], a comparison with the results of Rice [31] shall yet be executed.

3.6.1 Theoretical results

Bilby and Swinden consider the transverse shear mode III for which σ, σ_y, ε_y and δ have the meaning of shear stresses, shear strains and shear displacements respectively. This we shall have in mind in this section. Furthermore, Bilby and Swinden take as the nominal stress the mean stress over the total cross section WB which is equal to the remotely applied stress. With this definition general yielding takes place at the stress $\sigma_y(1-a/W)$. According to our definition in section 3.3, we use as the nominal stress the mean stress over the ligament (W-a)B and σ shall denote this (shear) stress here. It is 1/(1-a/W) times greater than the Bilby-Swinden stress and general yielding takes place at $\sigma=\sigma_y$. The plastic zone length is then equal to the ligament length W-a. In order to obtain a better adjustment to the mode I conditions we replace the normalization factor $Gb/2\pi$ of Bilby and Swinden by the factor $Gb/2\pi(1-\nu)=Eb/4\pi(1-\nu^2)$.

$\delta/W\,\varepsilon_y$ versus a/W is plotted in Figure 12 for $\sigma=\sigma_y$ and $\sigma=\sigma_y/2$, and $\delta/a\varepsilon_y$ versus a/W is plotted in Figure 13 for the same values of σ. The curves for smaller values of σ cannot be taken from Figure 12 of the paper [7]

because the curves for a/W=const lie too near together. We have reproduced both dependences since each of them exhibits special features: $\delta/W\varepsilon_y$ has a maximum at a/W=1/3 for $\sigma=\sigma_y$ and a flat maximum at a/W 0.5 for $\sigma=\sigma_y/2$. This enables a clear decision whether our results with CT specimens correspond to those of Bilby and Swinden.

$\delta/a\varepsilon_y$ increases steadily with decreasing a/W and becomes infinite for $a/W \to 0$ and $\sigma \to \sigma_y$ as $\ln 1/(a/W)$. These curves enable a comparison of $\delta/a\varepsilon_y$ with the factor Z of proportionality between K_I and σ as shown in section 3.7.2.

Within less than 5% deviations the curves in Figure 12 allow for the description

$$\frac{\delta}{W\varepsilon_y} = f_1\left(\frac{\sigma}{\sigma_y}\right)\left(\frac{\sigma}{\sigma_y}\right)^2 \cdot \left(\frac{a}{W}\right) \frac{(1-a/W)}{(a/W)^{n_1}} \quad \text{for } \frac{a}{W} \gtrsim 0.1 \tag{14}$$

Numerically results

$$f_1(1) = 1.9\ ,\ n_1 = 0.5 \quad \text{for } \sigma/\sigma_y = 1 \tag{14a}$$

$$f_1(1/2) = 1.9\ ,\ n_1 = 0.25 \quad \text{for } \sigma/\sigma_y = 1/2 \tag{14b}$$

In this stress range is therefore f_1 = const and $n_1 = 0.5\sigma/\sigma_y$. We have presented these equations only to illustrate the manner of the influence of a/W on δ. They do not allow for a connection to the results of section 2.1 because they do not represent the correct behaviour for $a/W \to 0$.

3.6.2 Basic assumption on the transfer of the theoretical results to mode I loading

For the analysis of the behaviour of the materials in large structures containing cracks, the theoretical results for infinite bodies are usually used as a basis of interpretation. The reason is the assumption that a/W may be considered to be sufficiently small in such structures. As we shall outline in connection with the fracture test results we think that under many practical conditions the effective value of a/W could not be taken as very small and that therefore the influence of a/W should be taken into account.

We have then to examine the conditions under which the results for mode III loading can be transfered to mode I loading. We assume that the general yielding state is the proper reference state for all geometries and correspondingly the general yield stress σ_{gy} the proper reference stress. Accordingly all states with equal σ/σ_y should be equivalent states. One phenomenon supporting this assumption is the fact that the crack opening displacement increases with an essentially higher power of the stress beyond general yielding than before it. On the other hand, we assume that the theoretical results for mode III loading provide qualitatively correct the influence of a/W and of σ on δ if we replace σ/σ_y by σ/σ_{gy} and δ/ε_y by δ/ε_y^* where

$$\varepsilon_y^* = \sigma_{gy}/E = b_{gy}\varepsilon_y \tag{15}$$

ε_y^* is the elastic strain in a smooth specimen, loaded with the tensile stress $\sigma=\sigma_{gy}$, of a material with the same elastic modulus E as that under consideration. In order to accentuate that ε_{gy}^* is no materials constant as ε_y we have marked it by the star.

According to this basic assumption we expect that with reference to equation (14) the connection between δ,σ and a/W is given by

$$\frac{\delta}{W\varepsilon_{gy}^*} = f_2\left(\frac{\sigma}{\sigma_{gy}}\right) \cdot \left(\frac{\sigma}{\sigma_{gy}}\right)^2 \cdot \frac{a}{W} \cdot g_2\left(\frac{a}{W}\right) \tag{16}$$

or

$$\frac{\delta}{a\varepsilon_{gy}^*} = f_2\left(\frac{\sigma}{\sigma_{gy}}\right) \cdot \left(\frac{\sigma}{\sigma_{gy}}\right)^2 \cdot g_2\left(\frac{a}{W}\right) \tag{17}$$

A possible dependence of g_2 on σ/σ_{gy} we shall discuss in section 3.8. From these equations follows

$$\frac{\delta}{\delta_{gy}} = \frac{1}{f_2(1)} \cdot f_2\left(\frac{\sigma}{\sigma_{gy}}\right) \cdot \left(\frac{\sigma}{\sigma_{gy}}\right)^2 \tag{18}$$

δ/δ_{gy} should therefore be a function of σ/σ_{gy} only, independent of a/W. If equation (18) becomes proved true by the experimental results, then it is as well confirmed that the variables σ/σ_{gy} and a/W can be separated as that σ/σ_{gy} is the proper stress ratio. Under this aspect we shall now consider the experimental results.

3.6.3 Experimental results

The values of $\delta/W\varepsilon_{gy}^*$ and of $\delta/a\varepsilon_{gy}^*$ as obtained for $\sigma=\sigma_{gy}$ and for $\sigma=\sigma_{gy}/2$ are given in Table 1 and the corresponding points are marked in the Figures 12 and 13. For both stress ratios $\delta/W\varepsilon_{gy}^*$ decreases with increasing a/W qualitatively in the same manner as $\delta/W\varepsilon_y$ according to Bilby and Swinden. It would be of interest to examine whether the theoretically predicted decrease of $\delta/W\varepsilon_{gy}^*$ with decreasing a/W towards a/W=0 would be experimentally verified. We could not make such experiments hitherto because we have no testing machine with a proper equipment for the necessary high loads. We intend, however, to make ready a large machine for this purpose. The values of $\delta/W\varepsilon_{gy}^*$ and $\delta/a\varepsilon_{gy}^*$ for bending specimens of Hy100 and Hy130 steels (b_{gy}=1.2) according to Fields and Miller [29] are marked in Figures 12 and 13 by crosses.

The course of σ/σ_{gy} versus δ/δ_{gy} is presented in Figure 14. The curves are drawn with the values of σ_{gy} and δ_{gy} from Figure 8 and with the curves $\sigma=\sigma(\delta)$ belonging to them. We see from Figure 14 that the curves are independent of a/W, i.e., fall together in one curve up to general yielding at $\sigma=\sigma_{gy}$. Our concept is therefore verified. Beyond general yielding the curves split up with a/W and δ increases with an essentially higher power of σ/σ_{gy} than before.

From the equations (16) and (17) follow all other dependencies of interest by deduction. Equation (17) shows that the curves $(\sigma/\sigma_{gy})^2$ versus $\delta/a\varepsilon_{gy}^*$ split up with a/W and this is likewise the case for the curves $(\sigma/\sigma_y)^2$

versus $\delta/a\varepsilon_y$ for which the additional dependence of the constraint factor b on a/W comes into play. These remarks may be enough since the stress intensity factor-displacement curves claim a higher interest and these we shall consider now.

3.7 Stress intensity factor-displacement curves

3.7.1 Connection between K_I and σ

Usually the stress intensity factor K_I is connected with the load P by

$$K_I = \frac{YP}{B\sqrt{a}} \tag{19a}$$

The formulas for the calculation of Y in dependence of a/W are given in the standard tables. We wish to connect K_I with σ and put therefore

$$\sigma = \frac{Y^*P}{Ba} \tag{19b}$$

The values of Y* follow from the equations (11a-c). Furthermore, if we put

$$K_I = Z\sqrt{a}\,\sigma \tag{19c}$$

we obtain

$$Z = Y/Y^* \tag{20}$$

Z versus a/W is plotted in Figure 15 for 3PB-, 4PB- and CT- specimens. The values of Z differ somewhat for the three specimen goemetries but their dependence of a/W is the same.

3.7.2 Relation between $\delta/a\varepsilon^*_{gy}$ and K_I and its consequences

From Table 1 we see that the ratio $(\delta/a\varepsilon^*_{gy})/Z^2$ is independent of a/W. The mean values are

$$= 1.0 \pm 0.1 \quad \text{for } \sigma=\sigma_{gy} \tag{21a}$$

$$\frac{\delta}{a\varepsilon^*_{gy}Z^2} = 0.09 \pm 0.009 \text{ for } \sigma=\sigma_{gy}/2 \tag{21b}$$

The average deviation of 10% is low compared with the strong dependence of $\delta/a\varepsilon^*_{gy}$ and Z^2 of a/W. According to this result equation (17) can be written in the form

$$\frac{\delta}{a\varepsilon^*_{gy}} = f_3\left(\frac{\sigma}{\sigma_{gy}}\right)\cdot\left(\frac{\sigma}{\sigma_{gy}}\right)^2\cdot Z^2 \tag{22}$$

Numerically is

$$f_3(1) = 1\ ,\ f_3(1/2) = 0.63 \tag{23a,b}$$

With equation (19c) follows from equation (22)

$$\frac{\delta}{\varepsilon^*_{gy}} = f_3\left(\frac{\sigma}{\sigma_{gy}}\right)\cdot\left(\frac{K_I}{\sigma_{gy}}\right)^2 = f_3\left(\frac{K_I}{\sqrt{a}Z\sigma_{gy}}\right)\left(\frac{K_I}{\sigma_{gy}}\right)^2 \tag{24a,b}$$

If we assume that the T-stress approximation is valid up to $\sigma=\sigma_{gy}/2$ we obtain according to equation (5) with $\theta=70.5^0$

$$\frac{\delta}{\varepsilon^*_{gy}} = 0.28\left(1+0.63\frac{\sigma}{\sigma_{gy}}\right)\cdot\left(\frac{K_I}{\sigma_{gy}}\right)^2 \tag{25a}$$

$$= 0.28\left(1+0.63\frac{K_I}{\sqrt{a}Z\sigma_{gy}}\right)\cdot\left(\frac{K_I}{\sigma_{gy}}\right)^2 \tag{25b}$$

The initial slope of the curve $(K_I/\sigma_{gy})^2$ versus $\delta/\varepsilon^*_{gy}$ is

$$1/\beta(\text{LEA}) = 3.6 \tag{26}$$

If we finally relate σ on σ_y and δ on ε_y we obtain from the equations (24a,b)

$$\frac{\delta}{\varepsilon_y} = \frac{1}{b_{gy}}f_3\left(\frac{\sigma}{b_{gy}\sigma_y}\right)\cdot\left(\frac{K_I}{\sigma_y}\right)^2 = \frac{1}{b_{gy}}f_3\left(\frac{K_I}{b_{gy}\sqrt{a}Z\sigma_y}\right)\cdot\left(\frac{K_I}{\sigma_y}\right)^2 \tag{27a,b}$$

With the mean value $b_{gy}=1.4$ results

$$1/\beta(\text{LEA}) = 5 \tag{28}$$

The experimental results are presented in the Figures 16a,b and 17a,b for the SSYR and for the macroscopic yielding range.

3.8 Discussion and Conclusions

The lines with the slopes (26) and (28) are drawn in the Figures 16a and 17a respectively. The slopes of the curves are initially much higher but take the values (26) and (28) already at $(\sigma/\sigma_{gy})^2\sim 0.06$ and $\delta/\delta_{gy}\sim 0.02$. We ascribe these steep initial parts to the residual compression stresses connected with the plastic zone of the fatigue crack. Such stresses cannot be avoided in this low strength steel even if the fatigue crack is produced at low temperatures and if the load is taken as low as possible. If the origin of a curve is shifted to the point at which the curve has the slope (26) or (28) the curve is described by equation (25b) or the corresponding equation for δ/ε_y up to $\sigma/\sigma_{gy}=1/2$. Thereby is expressed that the T-stress approximation is indeed applicable in this stress range. Some deviations exist between the experimental curves and the calculated ones. This is because we have used in the equations the mean value of $\delta/a\varepsilon^*_{gy}K_I^2$ whereas the experimental curves result with the values of Table 1. In view of the general feature of the curves, consisting in their split-up with a/W, from these differences can be disregarded in the SSYR. The split-up is relatively small up to general yielding for a/W=0.69 but becomes large for higher stresses because general yielding begins at different values of (K_I/σ_{gy}) or (K_I/σ_y) at different values of a/W.

The line with the slope 2 in Figure 17b demonstrates that in a wide range below general yielding the average slope of the curves has this value. Frequently this statement is considered as a confirmation of the theoretical prediction (6a). A view on Figure 2 shows, however, that in this range the plastic zone length is comparable with the crack length, i.e., this range is by no means the SSYR. In the actual SSYR range the slope has, according to our results, values between 5 and 4 and this result can be explained without constraint by the influence of the strain hardening according to Figure 6. We consider the general result of section 2.1, namely that the T-stress approximation is the correct approximation in the SSYR, to be essential in this respect. On the basis of a fourth order deviation from the LEA incorrect conclusions may be drawn.

The curves in the Figures 14, 16 and 17 have been obtained by means of selected curves $\sigma=\sigma(V_S)$ as pointed out in the sections 3.5 and 3.6.3. With the points which we have taken at first on the curves in Figure 8, the curves in Figure 14 did not fall together as well as shown in this Figure. They had, however, all the common features to bend-off quickly at a certain point lying near to the point (1,1). A slight correction of δ_{gy} was sufficient to shift this point to (1,1). The values of $\delta_{gy}/W\varepsilon^*_{gy}$ obtained in this way exhibited at the same time the general dependence on a/W as predicted by the theory and as shown in Figure 12. It is therefore possible to choose σ_{gy} and δ_{gy} in such a way that they fulfil all conditions in question. The values of σ_{gy} and δ_{gy} determined in this way for all measured curves in Figure 8 provide curves σ/σ_{gy} versus δ/δ_{gy} which slightly deviate only from the curves in Figure 14, but of course, with a scatter of the curves in the Figures 16 and 17 similar to that in Figure 8. These connections shall be represented in detail together with the results of the fracture experiments.

According to the dependence of n_1 in equation (14) on σ/σ_{gy} it could be expected that the function g_2 in equation (16) would depend on σ/σ_{gy}, too. This influence of σ/σ_{gy} is, however, weak in equation (14) and it disappears in the equations (16) and (17) because $\delta_{gy}/\delta(1/2)$ has the fixed value 10.9 ± 0.1 independent of a/W as follows from the values in Table 1. It would be of interest to examine whether this result remains true for smaller values of a/W.

Summarizing, we conclude from our results that the concept of the equivalence of the general yielding states is well confirmed. It provides an understanding of the curves in the Figures 16 and 17 and may be useful for the interpretation of the results of the fracture tests with respect to the COD concept. A high significance we ascribe to the theoretical results of the third order deviation from the LEA which suggests a re-examination of SSY behaviour of the materials.

4. EVALUATION OF THE FRACTURE TOUGHNESS FROM SMALL SPECIMEN DATA

Because of the scientific and economical significance of this problem it has found a wide interest. The research is based either on the COD concept [32], or the local fracture stress concept [33], or the concept of the local deformation work [34], or on a modified energy balance criterion [35].

We intend to go the following way for the interpretation of the results of our current tests [36]. Griffiths and Owen [37] have performed a finite element calculation for notched bending specimens with a notch radius

of 0.25 mm and a notch flank angle of 45^0 (such specimens we use in our experiments). Besides other relations Griffiths and Owen present the plastic zone length in the x-direction of Figure 1 (all other indices refer to the coordinate system of this Figure) and the stress intensification factor σ_{yymax}/σ_y as functions of the stress ratio σ/σ_{gy}. With the concept that the fracture occurs at a fixed value $\sigma_{ymax} = \sigma^*_f$ the authors find that σ^*_f is indeed nearly independent of the temperature. It seems, however, that from about 160K to about 110K, at which temperature the transition from the slip nucleated to the twin nucleated fracture takes place, σ^*_f increases slightly and then decreases somewhat down to 77K, the lowest test temperature (these properties we shall discuss in our workshop lecture). Rice and Johnson [38] and Ritchie et al., [33], have shown that the values of K_{Ic} evaluated on the basis of the σ^*_f concept agree in a wide temperature range with the measured values under the condition that σ_{yy} exceeds σ^*_f within a critical distance x_c from the crack tip. For the investigated steel with a grain size d=60µm resulted x_c = 120µm = 2d. In a recent investigation Curry and Knott [39] have extended this result to different grain sizes and have found that x_c has a rather constant value of about 180µm up to d ~ 50µm and then increases proportional to d.

We intend to examine whether this course of x_c shall be verified by our experimental results. If this should be the case we think that this method would merit some attention. We shall, however, additionally take into consideration the concept of Tetelman et al., [40] to replace the notch radius by an effective radius adapted to the conditions near a crack and the theoretical conceptions of Yokobori et al., [41] on the mechanism of the fracture.

ACKNOWLEDGEMENTS

We wish to express our many thanks to the Deutsche Forschungsgemeinschaft and to the European Community for Coal and Steel for financial assistance and to Dr. P. Neumann for valuable suggestions.

REFERENCES

1. NEUMANN, P., Constitutive Equations in Plasticity, ed. A.S. Argon, MIT Press, Cambridge, Mass., 1975, 449.
2. NEUMANN, P., Acta Met. 22, 1974,1155 and 1167.
3. DUGDALE, D.S., J. Mech. Phys. Solids 8, 1960, 100.
4. BARENBLATT, G.I., Problems of Continuum Mechanics (dedicated to the 70th birthday of N.I. Muskhelishvili), Soc. Industr. and Appl. Math., Philadelphia, Pa., 21, 1961. Advances in Applied Mechanics, 7, 1962, 55.
5. BILBY, B.A., COTTRELL, A.H. and SWINDEN, K.H., Proc. Roy. Soc. Lond., A272, 1963, 304.
6. RICE, J.R., J. Mech. Phys. Solids 22, 1974, 17.
7. BILBY, B.A. and SWINDEN, K.H., Proc. Roy. Soc. Lond. A285, 1965, 22.
8. VITEK, V., to be published in J. Mech. Phys. Solids, 1976.
9. RIEDEL, H., to be published in J. Mech. Phys. Solids, 1976.
10. ATKINSON, C., Internat. J. Fracture Mech. 2, 1966, 567.
11. MUSKHELISHVILI, N.I., Singular Integral Equations, Nordhoff, Groningen, 1953.
12. SMITH, E., Internat. J. Fracture Mech. 10, 1974, 61.
13. LINDLEY, T.C., Acta Met. 14, 1966, 1835. LINDLEY, T.C. and RICHARDS, C.E., Acta Met. 18, 1970, 1127. BRINDLEY, B.J. and LINDLEY, T.C., J. Iron Steel Inst. 210, 1972, 124.

14. SMITH, E., Internat. J. Fracture Mech. 4, 1968, 131.
15. REIFF, K. and LUECKE, K., Archiv Eisenhuettenwes, 46, 1975, 741.
16. COTTRELL, A.H., Trans. AIME 212, 1958, 192.
17. LEIBRFRIED, G., Zeitschr. Phys. 130, 1951, 214.
18. ESHELBY, J.D., FRANK, F.C. and NABARRO, F.R.N., Phil. Mag. 42, 1951, 351.
19. KOCHENDOERFER, A., SCHULZE, H.D. and RIEDEL, H., Internat. J. Fracture Mech. 11, 1975, 365.
20. RIEDEL, H., Nucleation and Propagation of cleavage microcracks, Proc. of the Internat. Conf. on Strength of Metals and Alloys, Nancy, France, August 30th to September 3rd, 1976.
21. PELLOUX, R.M.N., ASM Trans. Quart. 62, 1969, 1.
22. LARSSON, S.G. and CARLSSON, A.J., J. Mech. Phys. Solids 21, 1973, 263.
23. RICE, J.R. and TRACEY, D.M., Numerical and Computational Methods in Structural Mechanics, ed. S.J., Fenves, Perrone, N., Robinson, A.R. and Schonobrich, W.C., Academic Press, New York, 1973, 385.
24. SCHULZE, H.D., KOCHENDOERFER, A. and BAUER, G., Archiv Eisenhuettenwes. 45, 1974, 271.
25. SCHULZE, H.D. and KOCHENDOERFER, A., Archiv. Eisenhuettenwes, 45, 1974, 271.
26. KOCHENDOERFER, A. and SCHUERENKAEMPER, A., Archiv Eisenhuettenwes, 45, 1974, 271.
27. SCHMIDTMANN, E., RUF, P. and THEISSEN, A., Materialpruefung, 16, 1974, 343.
28. SCHMIDTMANN, E. and RUF, P., Archiv Eisenhuettenwes, 47, 1976, 95.
29. FIELDS, B.A. and MILLER, K.J., to be published in Eng. Fracture Mech., 1976.
30. EGAN, G.R., Eng. Fracture Mech. 5, 1973, 167.
31. RICE, J.R., Internat. J. Fracture Mech. 2, 1966, 426. Fracture Vol. II, Mathematical Fundamentals, ed. H. Liebowitz, Academic Press, New York and London, 1968, 191.
32. ROBINSON, J.N. and TETELMAN, A.S., ASTM Spec. Techn. Paper, 559, 1973, 139.
33. RITCHIE, R.O., KNOTT, J.F. and RICE, J.R., J. Mech. Phys. Solids 21, 1973, 395.
34. GILLEMOT, L.F., Eng. Fracture Mech. 8, 1976, 239. HAVAS, J., SCHULZE, H.D., HAGEDORN, K.E. and KOCHENDOERFER, A., Materialpruefung, 16, 1974, 349.
35. AURICH, D., Report on the 6th meeting of the working group, Fracture Processes, 1974, 85.
36. SCHULZE, H.D. and KOCHENDOERFER, A., presented at the meeting of the Deutsche Gesellschaft fuer Metallkunde, Nuernberg, 20th to 24th May, 1975.
37. GRIFFITHS, J.R. and OWEN, D.R.J., J. Mech. Phys. Solids, 19, 1971, 419.
38. RICE, J.R. and JOHNSON, M.A., Inelastic behaviour of solids, ed. M.F. Kanninen, W. Adler, A. Rosenfield and R. Jaffe, McGraw Hill, New York, 1970, 641.
39. CURRY, D.A. and KNOTT, J.F., Metal Science 10, 1976, 1.
40. TETELMAN, A.S., WILSHAW, T.R. and RAU, C.A., Internat. J. Fracture Mech. 4, 1968, 147.
41. YOKOBORI, T., KAMEI, A. and KONOSU, S., Internat. J. Fracture, 10, 1974. 375.

TABLE 1 - Room temperature values of the quantities for $\sigma=\sigma_{gy}$ and $\sigma=\sigma_{gy}/2$ of 2CT specimens, W=100 mm, of the investigated steel R St 37-2, yield stress σ_y = 237 MPa, elastic yield strain $\varepsilon_y=1.15\cdot10^{-3}$.

$\frac{a}{W}$ -	σ_{gy} MPa	$V_{s,gy}$ mm	δ_{gy} µm	b_{gy} -	ε^*_{gy} 10^{-3}	$\frac{\delta_{gy}}{W\varepsilon^*_{gy}}$ -	$\frac{\delta_{gy}}{a\varepsilon^*_{gy}}$ -
0.32	291	1.23	127	1.23	1.41	0.90	2.8
0.53	354	1.22	108	1.49	1.72	0.63	1.2
0.69	362	1.10	47	1.53	1.76	0.27	0.4

$\frac{a}{W}$ -	$\delta(\frac{1}{2})$ µm	$\frac{\delta(\frac{1}{2})}{W\varepsilon^*_{gy}}$ -	$\frac{\delta(\frac{1}{2})}{a\varepsilon^*_{gy}}$ -	z^2 -	$\frac{\delta_{gy}}{a\varepsilon^*_{gy}z^2}$ -	$\frac{\delta(\frac{1}{2})}{a\varepsilon^*_{gy}z^2}$ -	$z\sqrt{\frac{a}{mm}}$ $\sqrt{mm}$
0.32	11.5	0.08	0.25	3.07	0.9	0.08	9.9
0.53	9.9	0.06	0.11	1.06	1.1	0.10	7.5
0.69	4.4	0.03	0.04	0.46	0.9	0.09	5.6

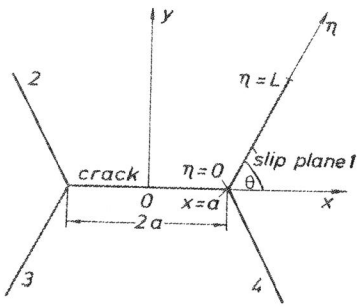

Figure 1 Coordinate systems for a crack with inclined slip planes in an infinite body.

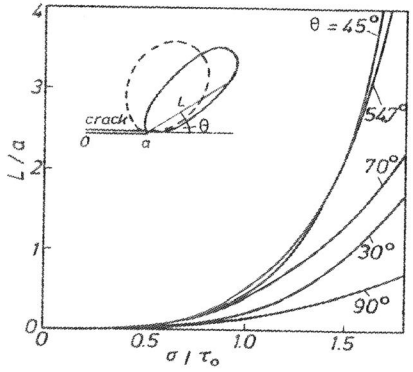

Figure 2 Normalized slip band length L versus normalized stress σ for various slip plane inclination angles θ. The inset shows the polar diagrams L(θ) with arbitrary units of L for small scale yielding (dashed line) and for large scale yielding with $\sigma=1.5\tau_o$ (full line).

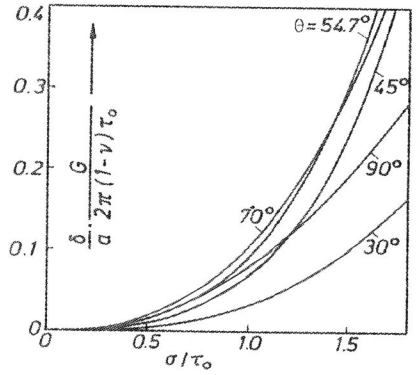

Figure 3 Normalized crack tip displacement δ versus normalized applied stress σ for various slip plane inclination angles θ.

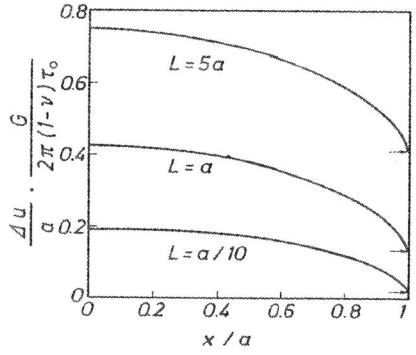

Figure 4 Crack profiles: normalized displacement Δu versus normalized distance x from crack tip for various slip band lengths L. Slip band inclination angle $\theta=45^0$.

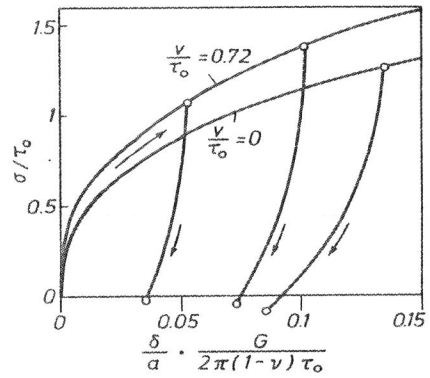

Figure 5 Normalized stress σ versus normalized crack tip displacement δ for loading and unloading, indicated by the arrows, without (v=0) and with ($v=0.72\tau_o$) strain hardening. Slip plane inclination angle $\theta=45^0$. The circles mark the incipient contacting of the crack faces.

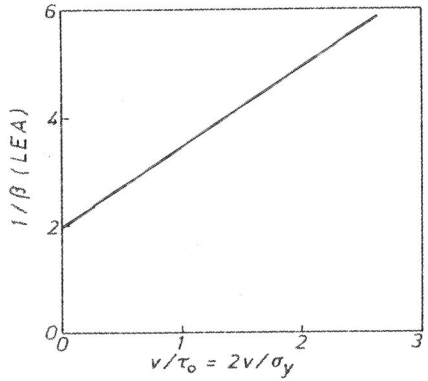

Figure 6 Linear elastic approximation slope $1/\beta$, equation (6), versus normalized strain hardening coefficient v. Slip plane inclination angle $\theta=70.5^0$.

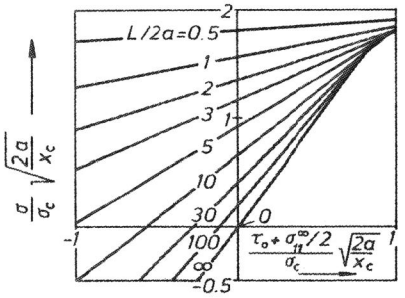

Figure 7 Normalized fracture stress σ versus normalized frictional shear stress τ_o for various slip band lengths L.Slip plane inclination angle $\theta=45^0$.

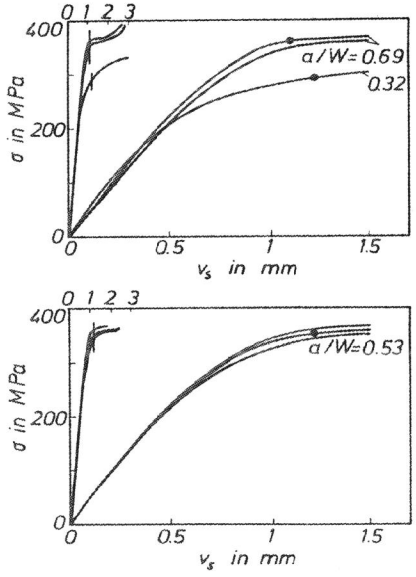

Figure 8 Nominal stress σ versus surface displacement V_S of 2CT specimens with the termed values of a/W. The curves on the left hand side (upper abscissa scale) are obtained with a low sensitive measuring device for V_S, the curves on the right hand side (lower abscissa scale) with a high sensitive device. The points marked by circles and the curves through them are used for the further evaluations.

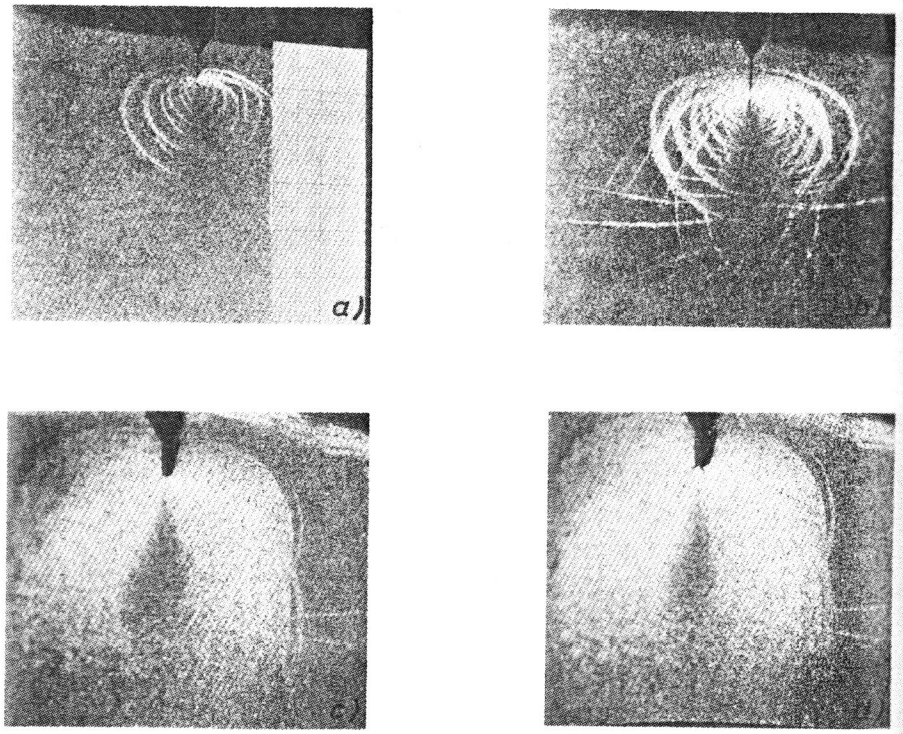

Figure 9 Photographs of the lacquer covered side surface of a 2CT specimen with a/W=0.53. At the top is the end of the machined slit, at the bottom the opposite specimen surface. The scale as indicated by the mm-grid in (a) is the same for all photographs. (a) partial scale yielding, σ=321 MPa, δ=84 μm; (b) near general yielding, σ=326 MPa, δ=130 μm; (c) macroscopic yielding, additional slip bands at the tip of the opened fatigue crack, σ=363 MPa, δ=1.7 mm; (d) advanced macroscopic yielding, beginning of the stable crack propagation by the right hand sided of the generated microcracks at the tip of the fatigue crack, σ=368 MPa, δ=2.8 mm.

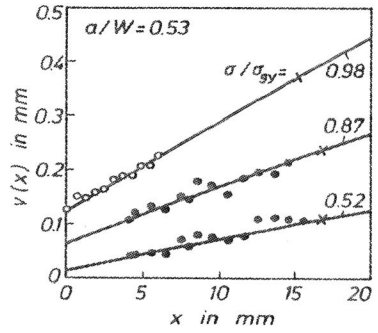

Figure 10 Surface displacement V_S versus distance x from the crack tip for the termed values of the nominal stress σ. The open circles mark the values obtained by microscopic measurement of the distance of the border lines of the crack from photographs as in Figure 9. The full circles mark the values obtained by measurement of the displacement of identations. The crosses mark the values for $x=x_1$.

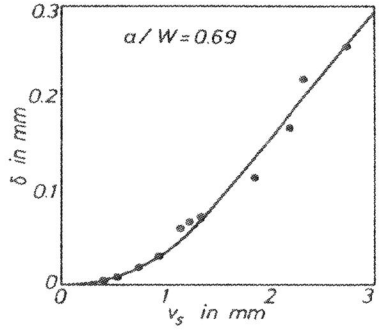

Figure 11 Crack tip displacement δ versus surface displacement V_S.

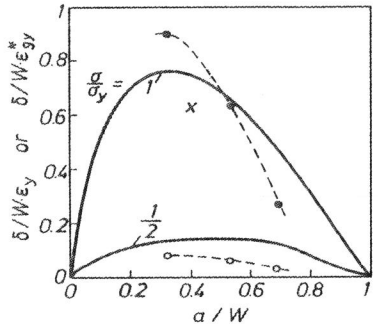

Figure 12 Crack tip displacement δ related to $W\varepsilon_y$ versus crack to specimen length ratio a/W for the termed values of the stress ratio σ/σ_y according to Bilby and Swinden [7] and 2CT specimen values of $\delta/W\varepsilon^*_{gy}$ for σ/σ_{gy}=1 (•) and σ/σ_{gy}=1/2 (o).

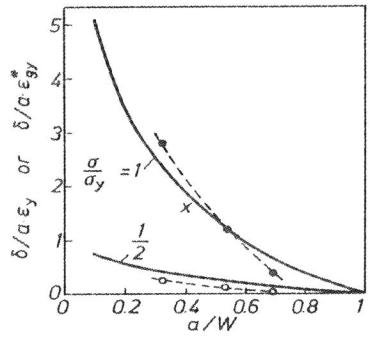

Figure 13 $\delta/a\varepsilon_y$ versus a/W according to Bilby and Swinden [7] and $\delta/a\varepsilon^*_{gy}$ of 2CT specimens. Further information in the legend to Figure 12.

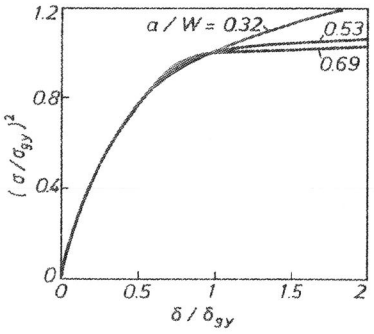

Figure 14 Stress ratio $(\sigma/\sigma_{gy})^2$ versus crack tip displacement ratio (δ/δ_{gy}) for 2CT specimens with the termed values of the crack to specimen length ratio a/W.

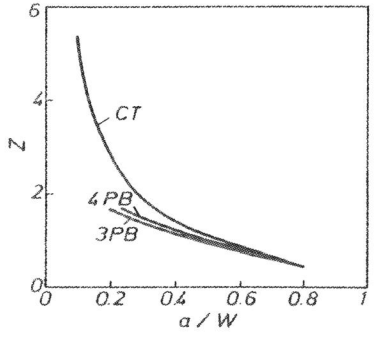

Figure 15 Proportionality factor Z between normalized stress intensity factor $K_I/\sqrt{a}$ and nominal stress σ versus crack to specimen length ratio a/W for three point bending (3PB)-, four point bending (4PB)- and CT-specimens.

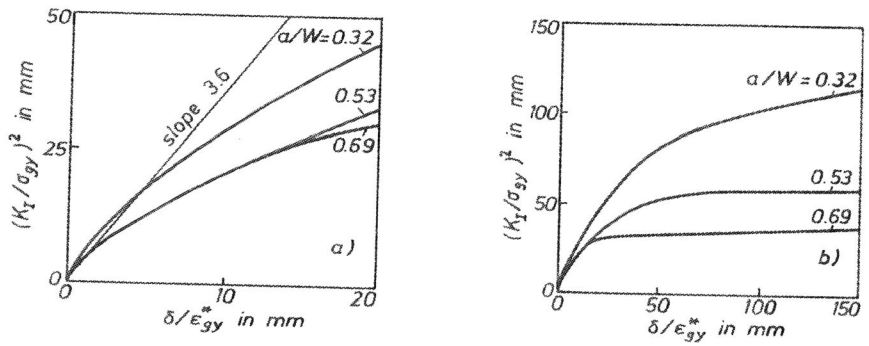

Figure 16 On general yielding quantities normalized square of the stress intensity factor K_I versus crack tip displacement δ of 2CT specimens with the termed values of the crack to specimen length ratio a/W. (a) small scale yielding range, (b) up to the macroscopic yielding range.

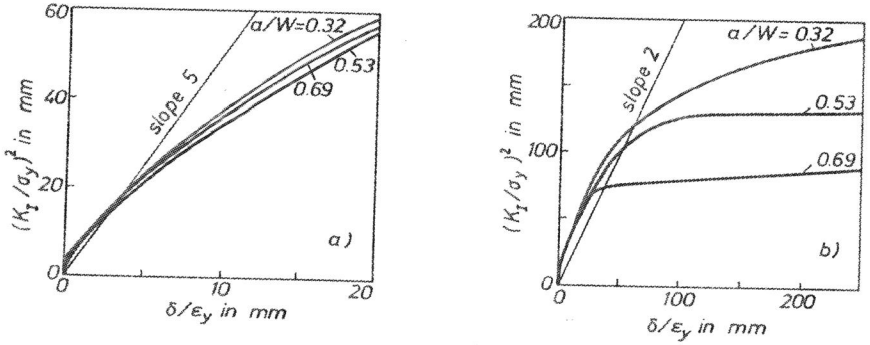

Figure 17 On uniaxial yielding quantities normalized square of the stress intensity factor K_I versus crack tip displacement δ of 2CT specimens. Otherwise as in Figure 16.